Part I

Overview

1

Main Objective

> Turbulence is one of the principal unsolved problems of physics today. ....The real challenge, it seems to us, is that no adequate model for turbulence exists today.... The equations of motion have been analyzed in great detail, but it is still next to impossible to make accurate quantitative predictions without relying heavily on empirical data. (Tennekes and Lumley in A First Course in Turbulence, 1994).

1.1 Computational Turbulent Incompressible Flow

This book is Vol 4 of the Body & Soul series and is devoted to *computational fluid dynamics* with focus on *turbulent incompressible flow*. In this first Part I we give a glimpse of the central themes of the book, which are developed in detail in Part II on mathematical aspects, Part III revealing secrets of fluid flow in basic applications, Part IV on computational aspects, Part V on fundamental aspects of fluid flow and a concluding Part VI leading into thermodynamics of turbulent compressible flow. In the forthcoming Vol 5 of the Body & Soul series, we continue to make a synthesis of incompressible and compressible fluid dynamics as *Computational Thermodynamics*.

A *fluid* may appear in the form of a liquid like water or a gas like air. Water is virtually *incompressible*; the relative change in volume for each atmosphere in pressure is less than 10^{-6}. Air can be viewed to be incompressible as long as the flow speed is well below the speed of sound, that is for flow speeds less than say 300 kilometers per hour (200 miles per hour).

Turbulence in fluid flow represents a basic phenomenon of our world of crucial importance in a wide range of phenomena in Nature and technical applications. Turbulent flow has a complex, seemingly chaotic, variation in space and time on a wide range of scales from small to large, and typically appears for fluids with *small viscosity*, such as air and water.

The basic mathematical models for fluid flow, incompressible and compressible, are given by the the *Euler equations* and the *Navier–Stokes equa-*

tions expressing conservation of mass, momentum and energy. The Euler equations model the flow of a fluid with zero viscosity, referred to as an *ideal fluid*, and were formulated by Euler in 1755. The Navier–Stokes equations model the flow of a fluid with positive viscosity, and were formulated during 1821-45 by Navier, Stokes, Poisson and Saint-Venant (Fig. 1.1), assuming the fluid to be *Newtonian*, with the viscous forces depending linearly on velocity strains.

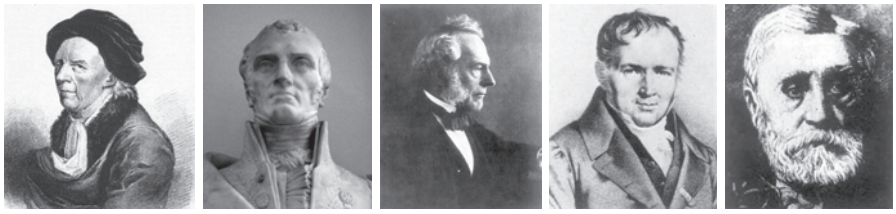

Fig. 1.1. Leonhard Euler (1707–1783), Claude Louis Marie Henri Navier (1785–1836), George Gabriel Stokes (1819–1903), Siméon Denis Poisson (1781–1840), and Adhémar Jean Claude Barré de Saint-Venant (1797–1886).

We all have practical experience of fluid motion and the concept of *viscosity* for fluids with large viscosity such as heavy oil or tooth paste, and fluids with small viscosity such as air and water. The Navier–Stokes equations appear to be an accurate mathematical model of fluid flow with varying viscosity from small to large, including in particular turbulent flow for fluids with small viscosity. There are also non-Newtonian fluids with a nonlinear dependence of the viscosity, typically fluids with large viscosity such as polymers.

The basic mathematical models for turbulence thus appear to be known since very long, but nevertheless turbulence is viewed as the basic open problem of classical mechanics. How can it be? The main reason is that the progress of solving the Navier–Stokes equations using analytical mathematical methods to obtain quantitative information about turbulent flow, has been very slow or rather non-existent, because the complexity of turbulent solutions to the Navier–Stokes equations defy analytical representations. Even basic qualitative mathematical questions concerning existence and uniqueness of solutions represent open problems seemingly inaccessible to analytical mathematical treatment using classical methods of calculus and functional analysis.

The main objective of this book is to show that it is possible to accurately simulate turbulent fluid flow by solving the Euler or Navier–Stokes equations computationally using solid mathematical principles, in simple geometries on a PC, and in complex geometries on clusters of PCs. The main objective is thus to demonstrate that *computational turbulence* now is available for massive use in a wide range of applications.

We will show that the objective may be reached by solving the Euler and Navier–Stokes equations using a *finite element method* which we refer to as *General Galerkin* or *G2* for short. G2 is a *Galerkin method* seeking a solution

in a finite element space with residual orthogonal to a set of finite element test functions combined with a *weighted least squares* control of the residual. G2 is *adaptive* with

- *automatic turbulence modeling*,
- *automatic error control*.

The adaptivity is based on solving a linearized dual problem to obtain sensitivity in output or quantities of interest in terms of the residual and the finite element mesh size.

As a preview of the book, below we present some G2 computations including solutions of associated linearized dual problems (Figs. 1.2–1.24).

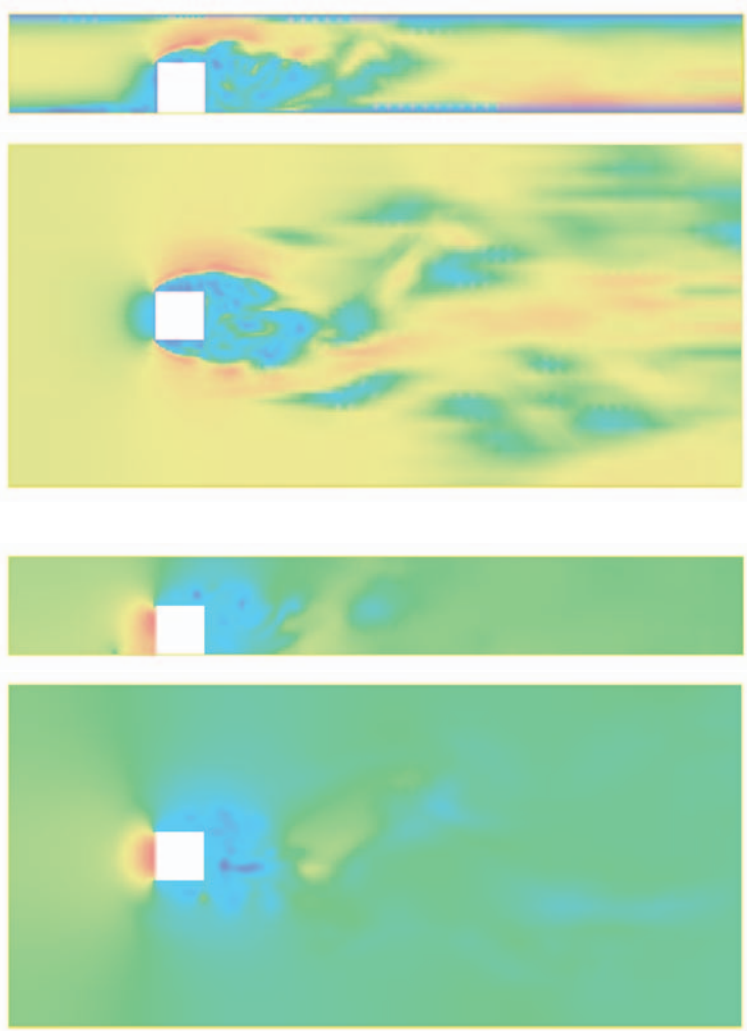

Fig. 1.2. From Chapter 15: Surface mounted cube: velocity $|U|$ (upper) and pressure P (lower), in the x_1x_2-plane at $x_3 = 3.5H$ and in the x_1x_3-plane at $x_2 = 0.5H$.

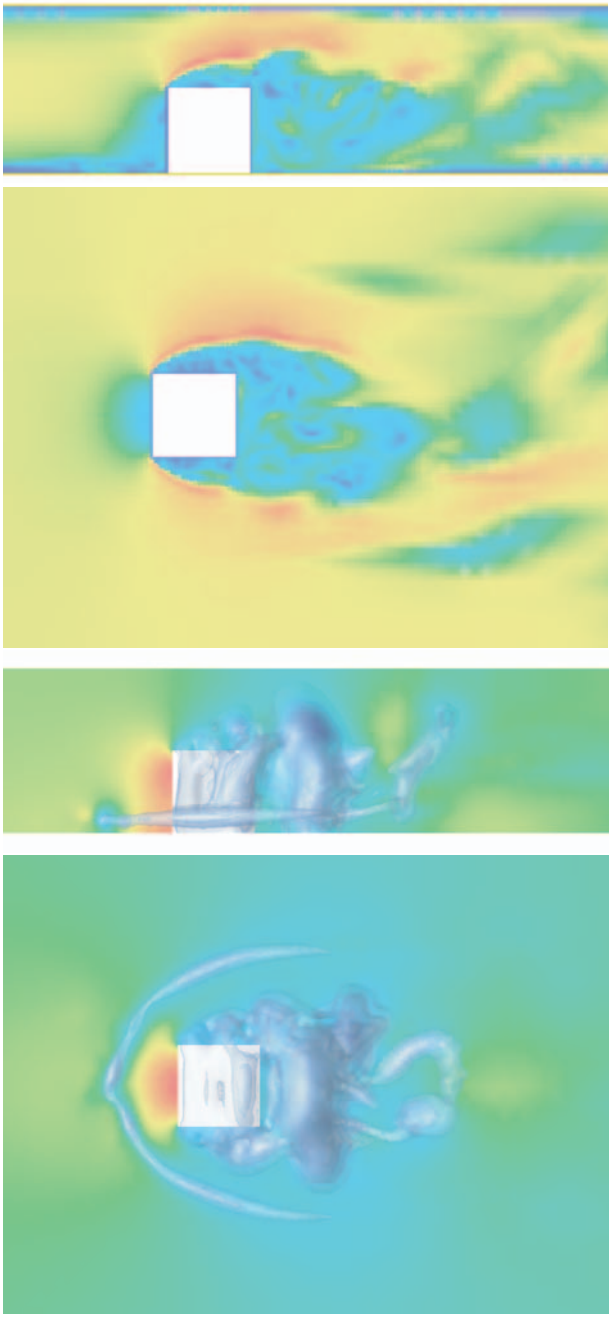

Fig. 1.3. From Chapter 33: Surface mounted cube: Magnitude of velocity (upper), and pressure color map, with iso-surfaces for negative pressure, illustrating the horse shoe vortex.

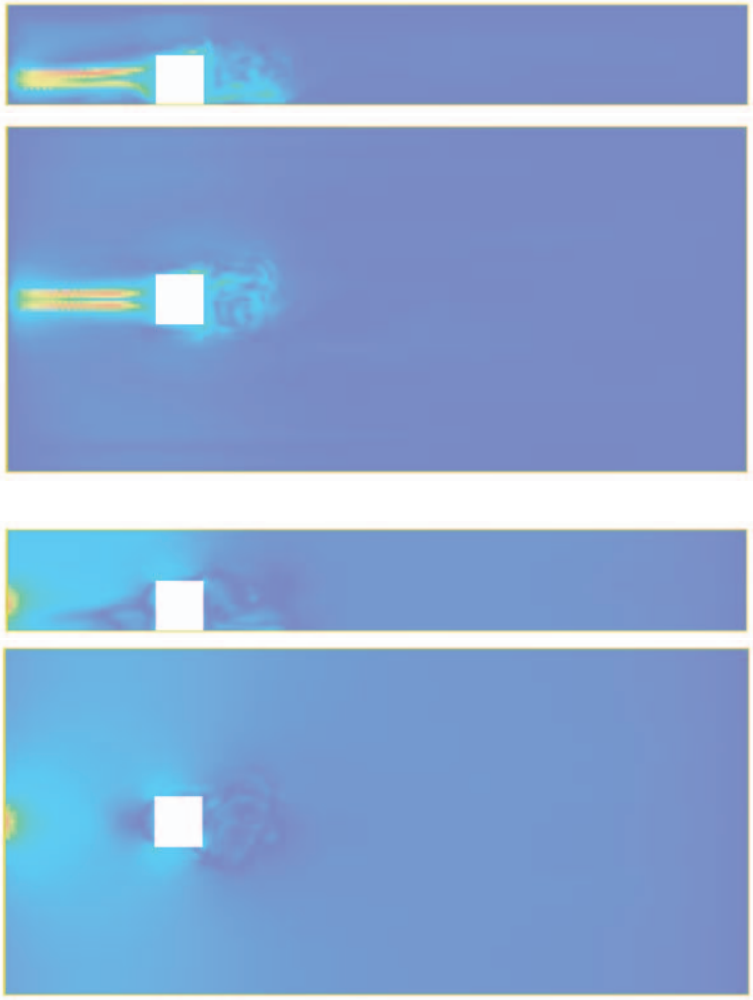

Fig. 1.4. From Chapter 15: Surface mounted cube: dual velocity $|\varphi_h|$ (upper), and dual pressure $|\iota_h|$ (middle), in the x_1x_2-plane at $x_3 = 3.5$H and in the x_1x_3-plane at $x_2 = 0.5$H.

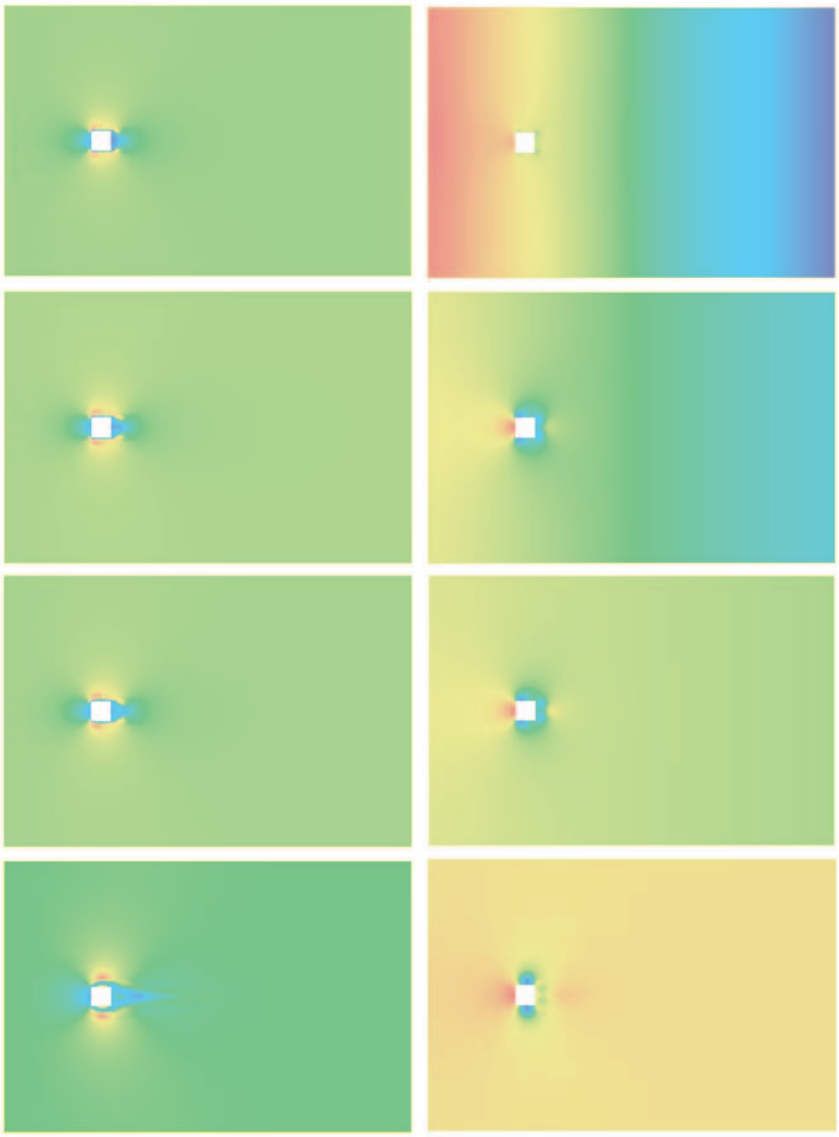

Fig. 1.5. From Chapter 19: Magnitude of the computed velocity (left) and pressure (right) corresponding to zero initial data, for time steps 4,6,8,32.

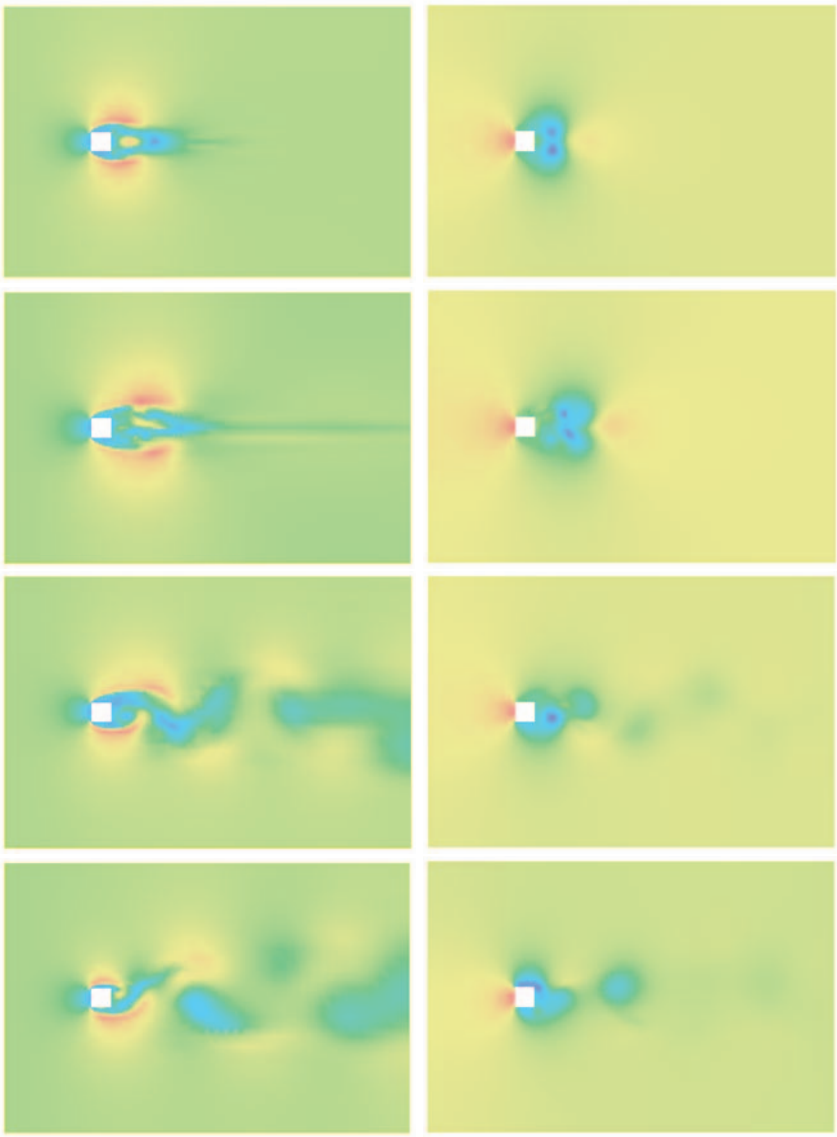

Fig. 1.6. From Chapter 19: Magnitude of the computed velocity (left) and pressure (right) corresponding to zero initial data, for time steps 64,128,704,1024.

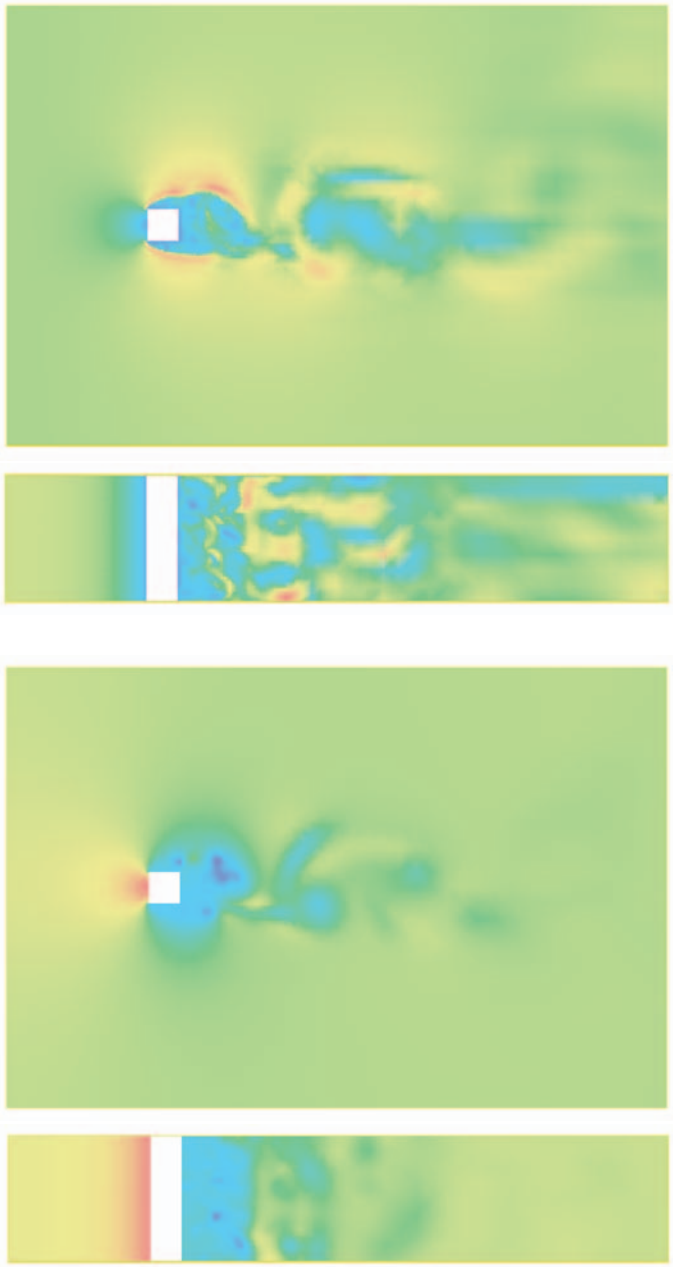

Fig. 1.7. From Chapter 33: Velocity $|U|$ (upper), and pressure P (lower), in the x_1x_2-plane at $x_3 = 2D$.

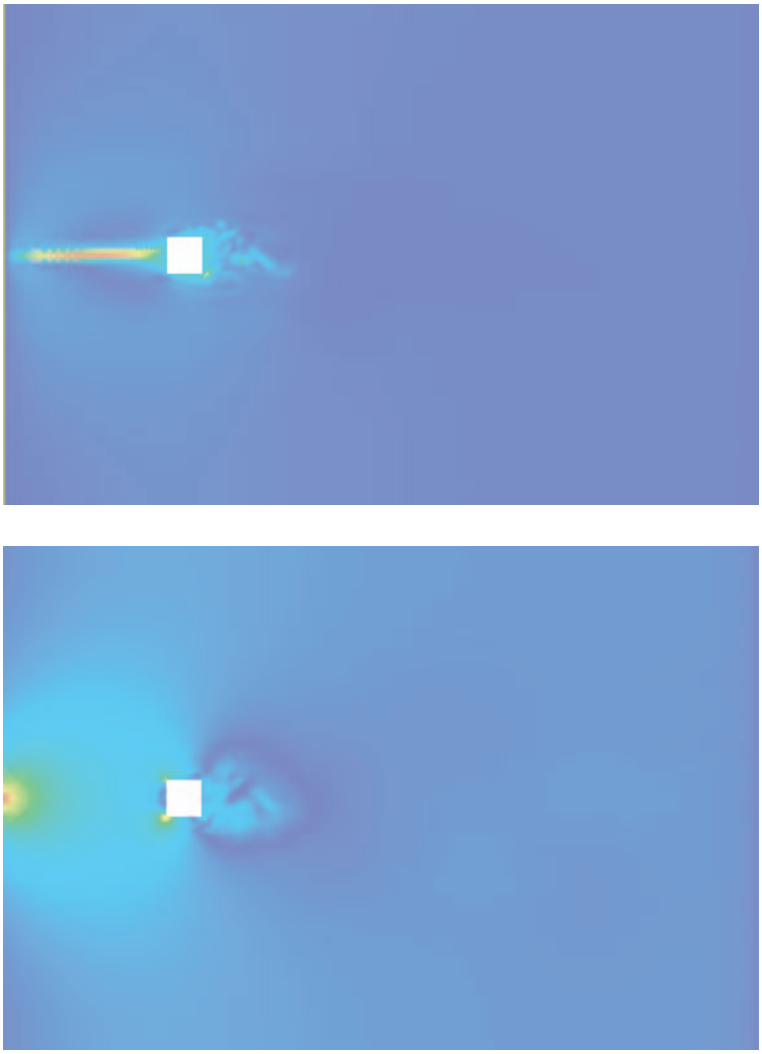

Fig. 1.8. From Chapter 33: Square cylinder: dual velocity $|\varphi_h|$ (upper), and dual pressure $|\iota_h|$ (lower), in the x_1x_3-plane at $x_2 = 7D$ and in the x_1x_2-plane at $x_3 = 2D$.

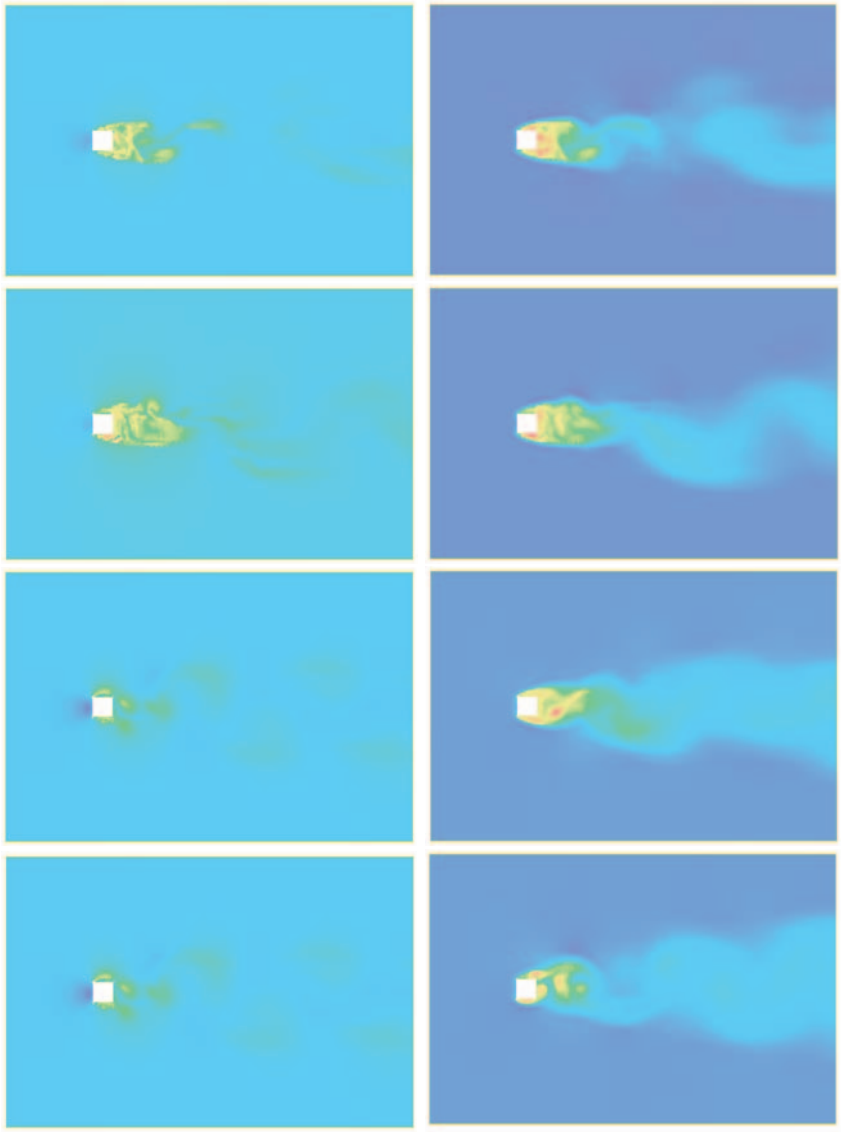

Fig. 1.9. From Chapter 19: Total energy e (left) and temperature T (right); $t = 4.5, 5.5, 11, 16$.

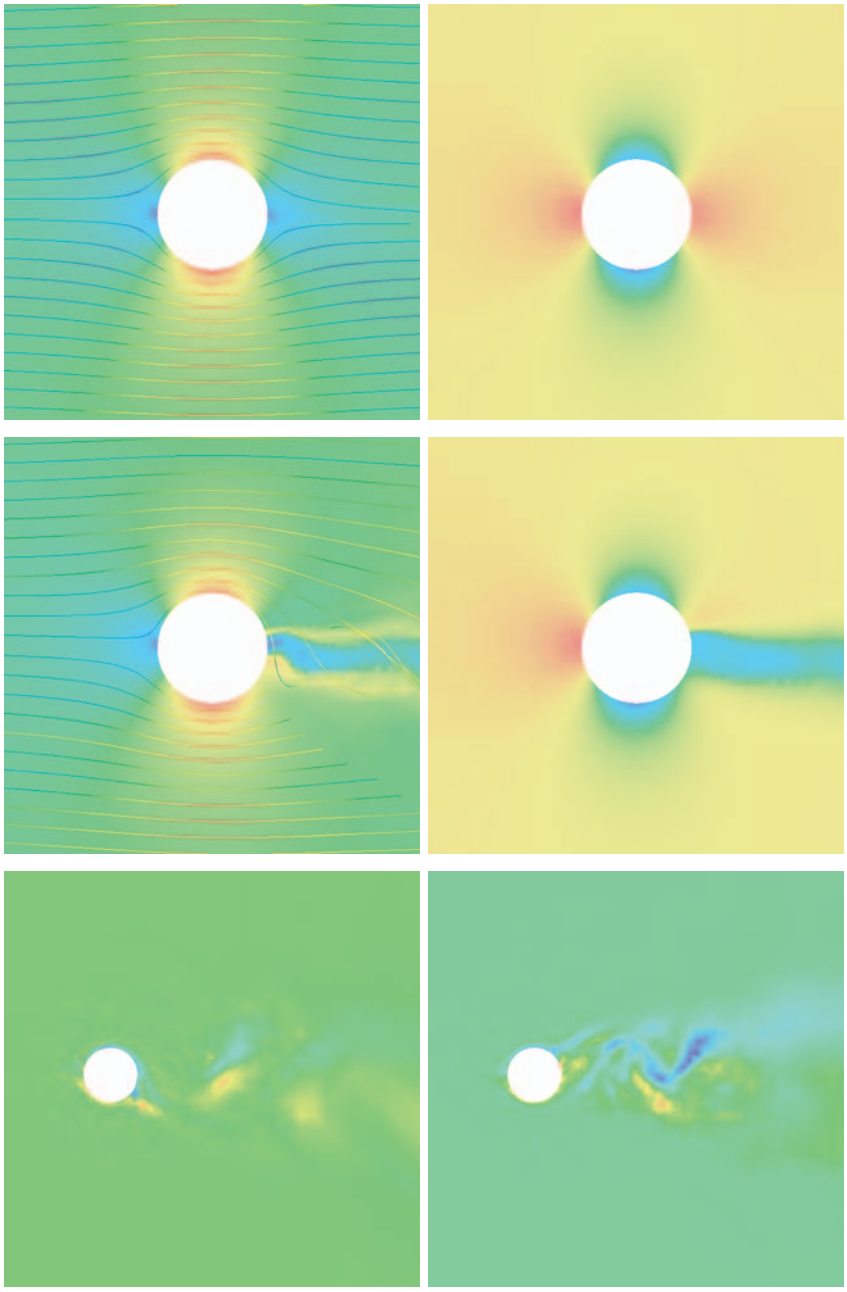

Fig. 1.10. From Chapter 12 and Chapter 35: Flow past a circular cylinder; velocity and pressure for the potential solution and a G2 turbulent solution (upper), and out of paper vorticity of the G2 solution at two different times, in two different sections parallel to the x_1x_2-plane (lower).

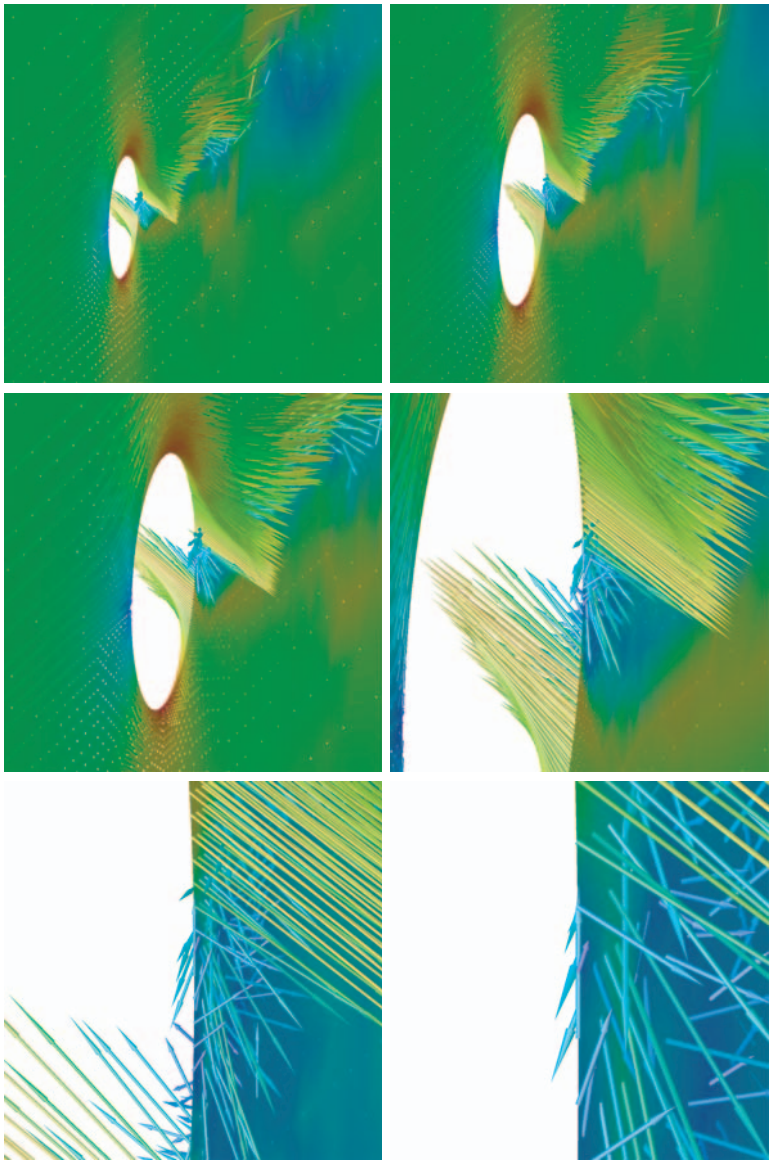

Fig. 1.11. From Chapter 12: Snapshot of the velocity in a G2 computation illustrating the single separation point.

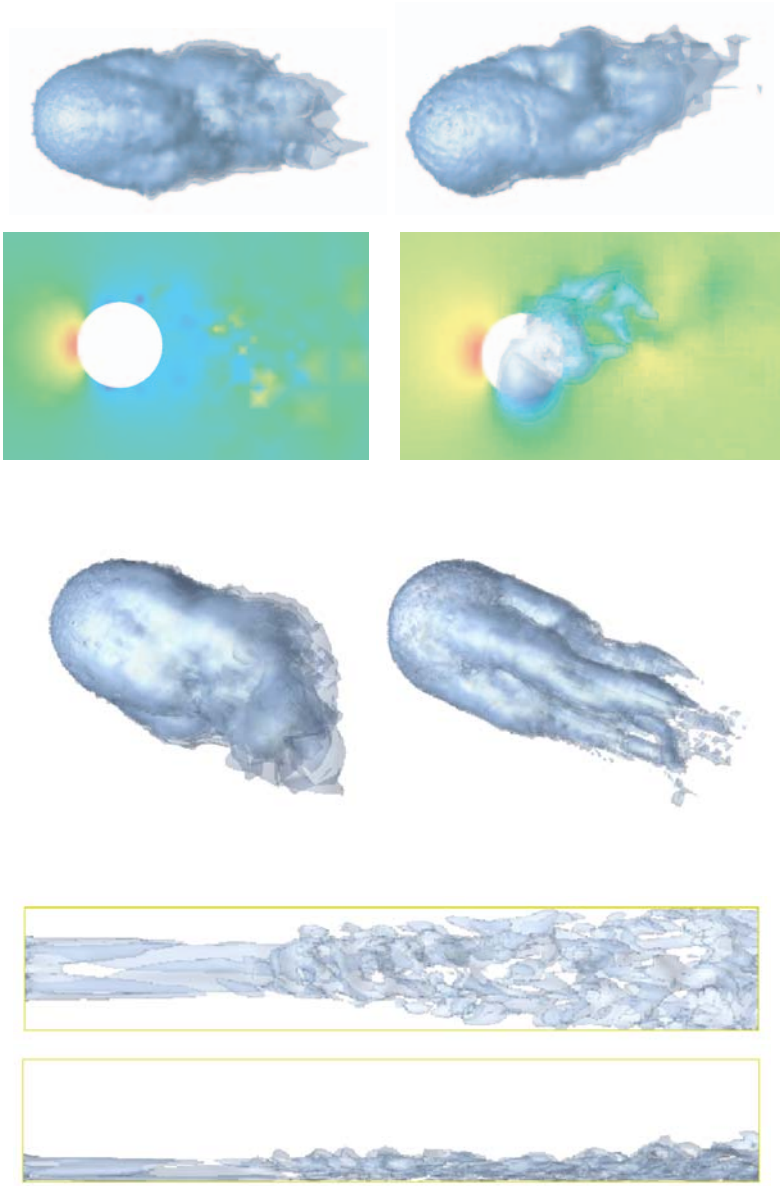

Fig. 1.12. From Chapter 21 and Chapter 36: Pressure for a still and a rotating sphere (upper), and vorticity for a sphere before and after drag crisis (middle), and transition to turbulence in a boundary layer computation (lower).

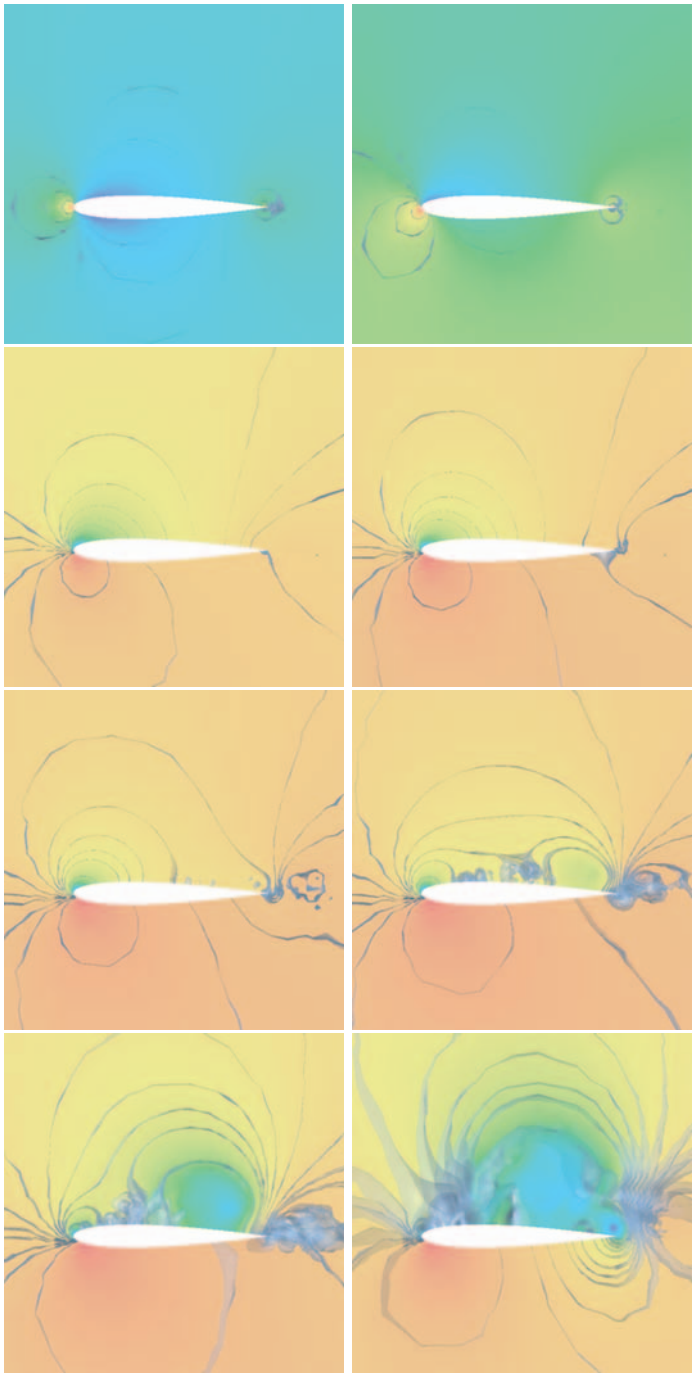

Fig. 1.13. From Chapter 22: Pressure for a 3d wing using EG2, with increasing angle of attack; 0,4,12,14,16,18,20, and 22°.

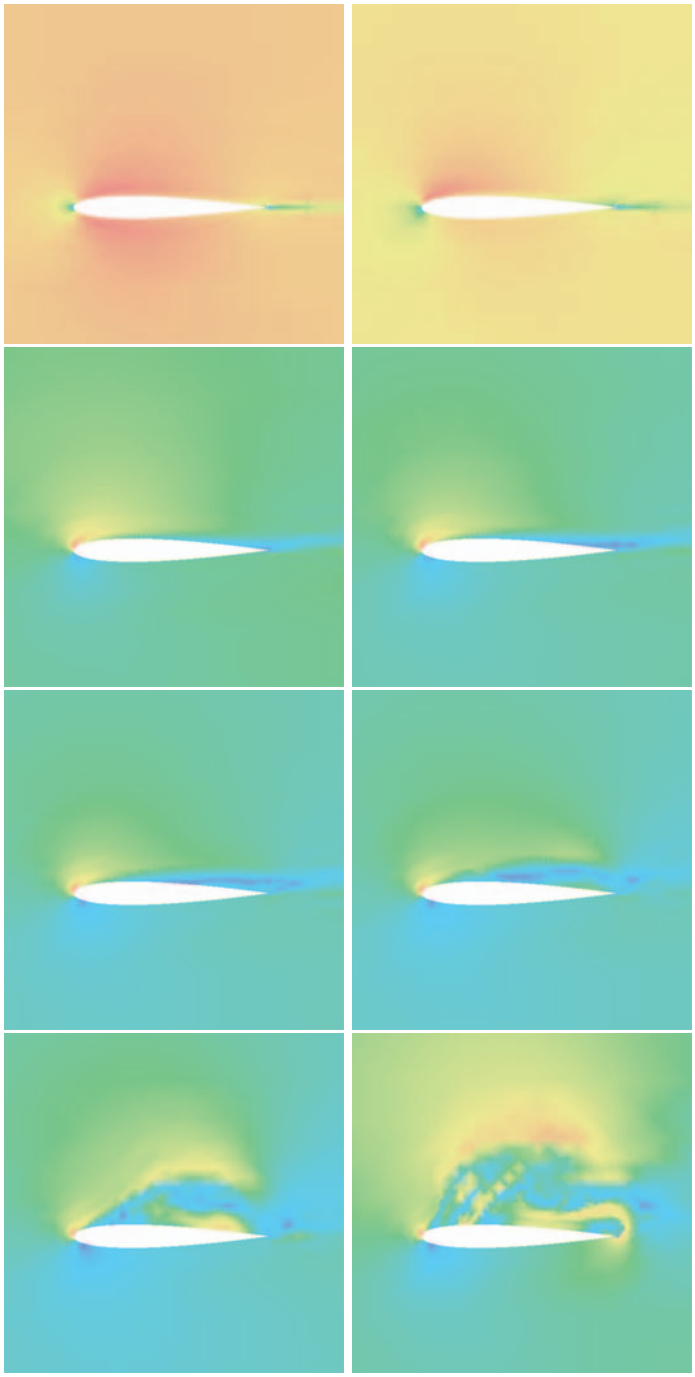

Fig. 1.14. From Chapter 22: Magnitude of the velocity for a 3d wing using EG2, with increasing angle of attack; 0,4,12,14,16,18,20, and 22°.

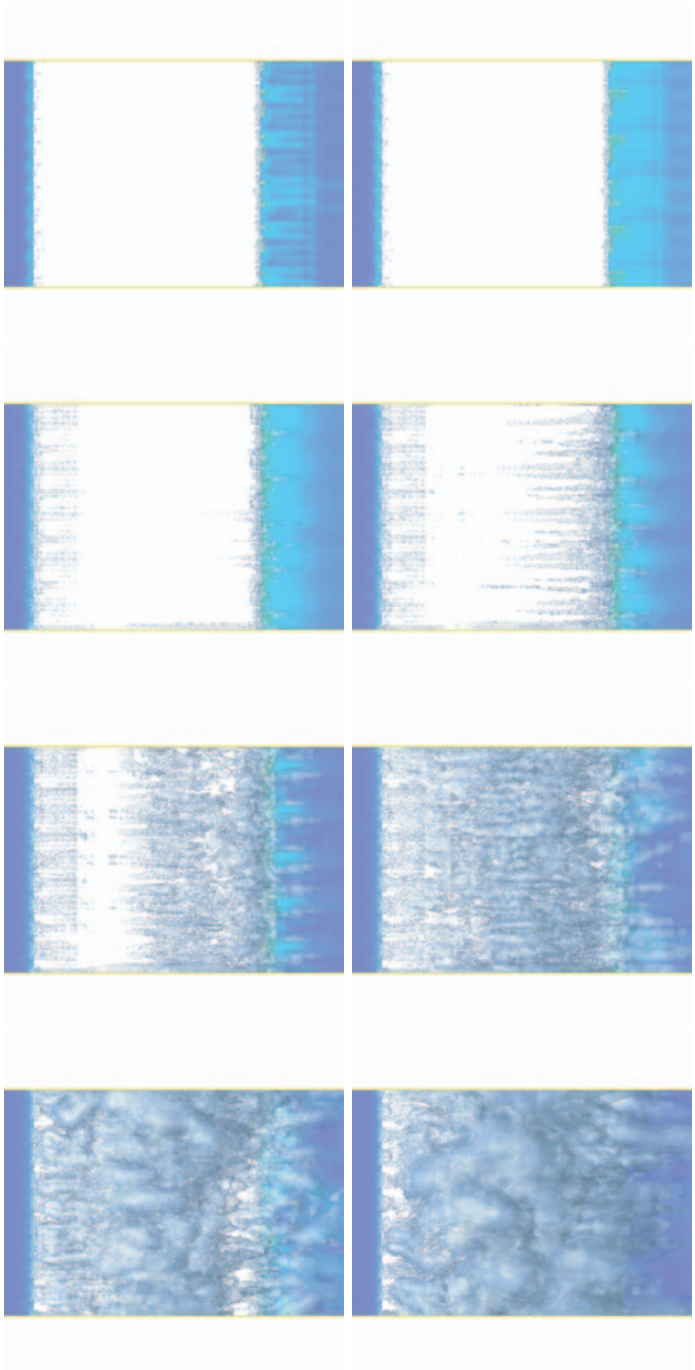

Fig. 1.15. From Chapter 22: Magnitude of first 2 vorticity components $|(\omega_1, \omega_2)|$ for a 3d wing using EG2 (with the third component in the direction of the wing), with increasing angle of attack; 0,4,12,14,16,18,20, and 22°.

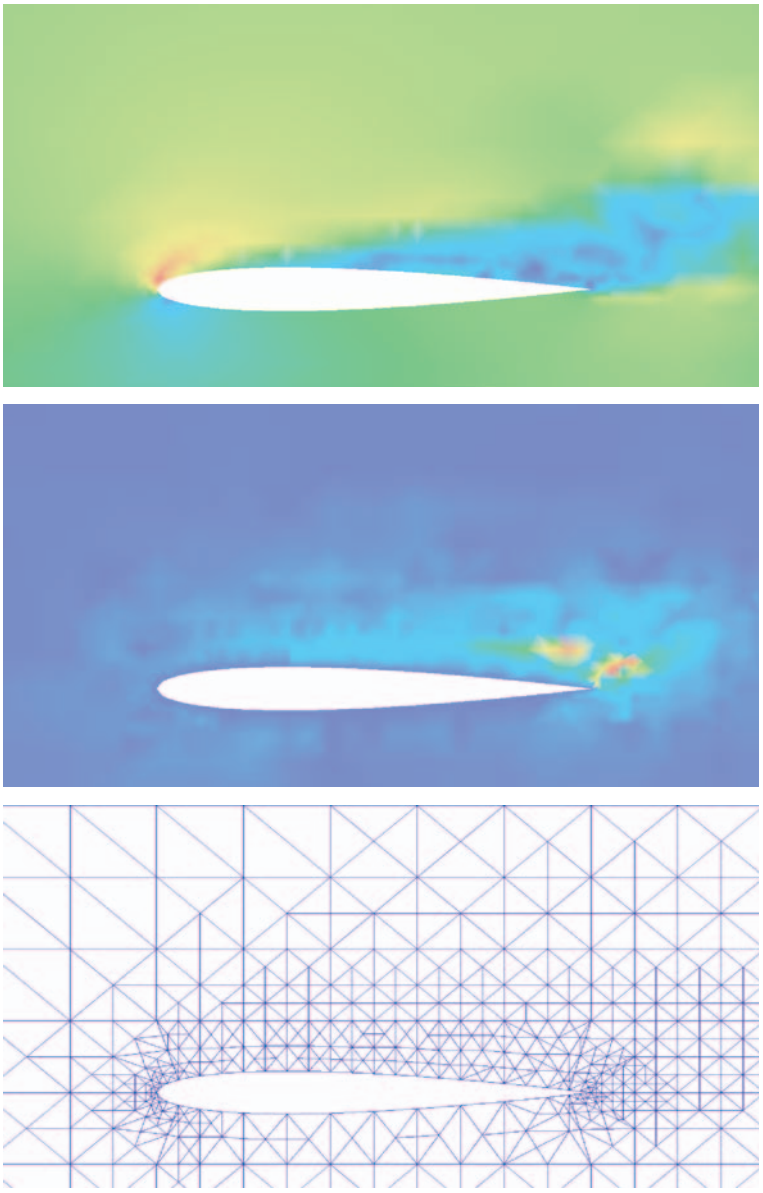

Fig. 1.16. From Chapter 35: Adaptive mesh refinement for the flow past a NACA 0012: magnitude of the velocity (upper), dual solution (middle) representing sensitivity information related to the computation of lift and drag, and a corresponding (coarse) mesh under refinement (lower).

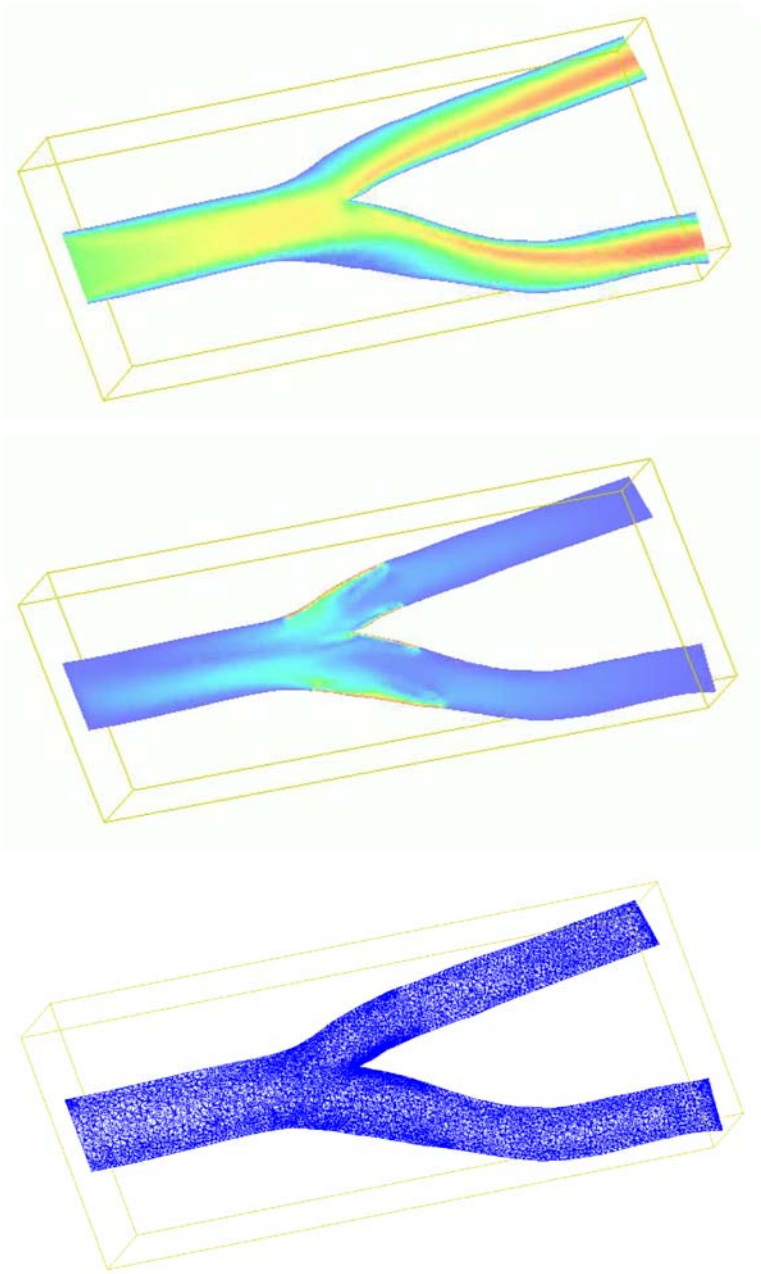

Fig. 1.17. From Chapter 35: Midsections showing snapshots of a G2 simulation of the blood flow in a realistic bifurcation model of a human carotid bifurcation (upper), the dual solution corresponding to the computational error in wall shear stress (middle), and the corresponding mesh (lower). Geometrical model produced by K. Perktold, TUG Graz, developed from an experimental cast (D. Liepsch, FH Muenich).

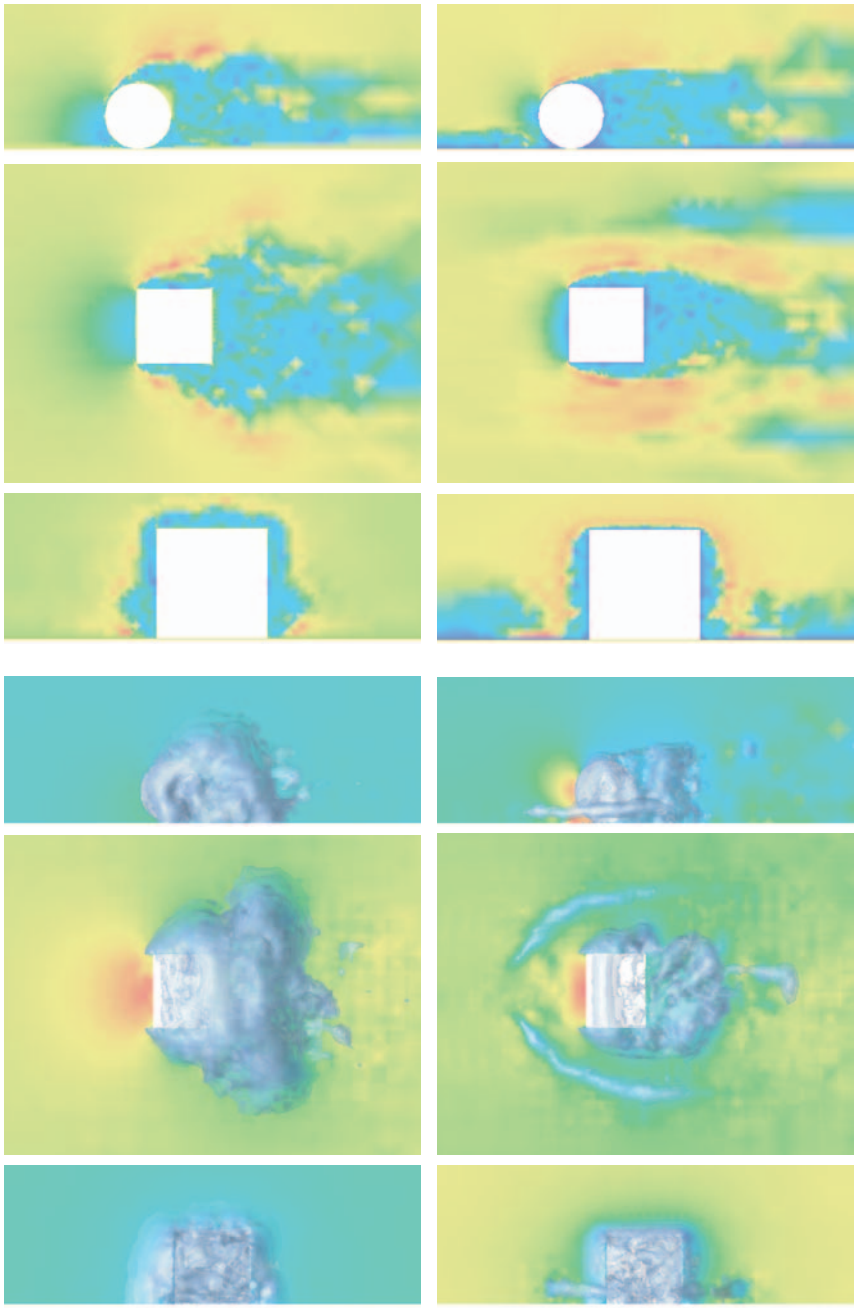

Fig. 1.18. From Chapter 35: Snapshots of magnitude of velocity (upper) and pressure and iso-surfaces of negative pressure (lower), for rotating (left) and stationary (right) cylinder, in the x_1x_2-, x_1x_3-, and x_2x_3-planes, through the center of the cylinder.

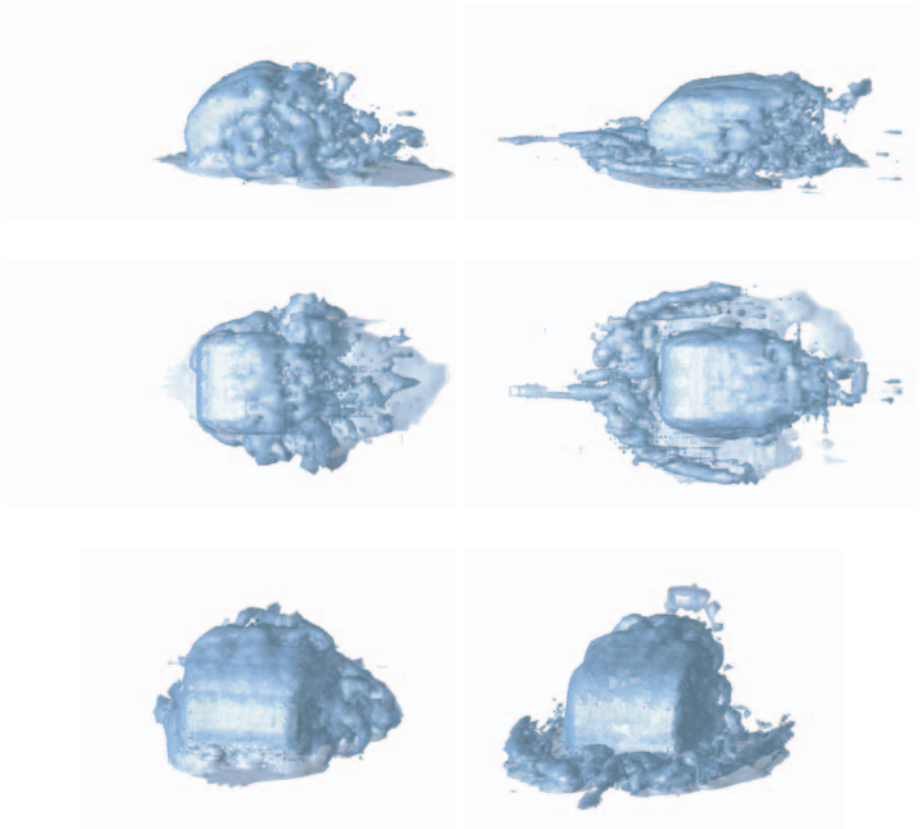

Fig. 1.19. From Chapter 24: G2 solutions of the flow past a wheel: snapshots of magnitude of the vorticity for the rotating (left) and the stationary (right) cylinder.

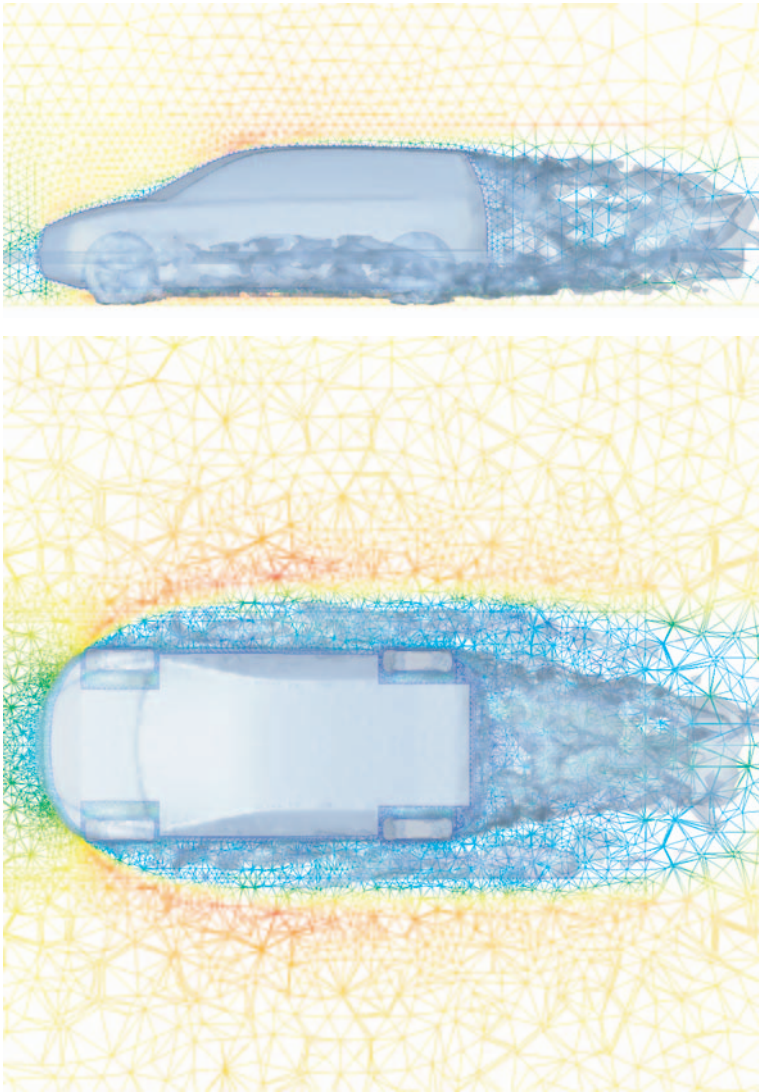

Fig. 1.20. From Chapter 33: G2 solution of the turbulent flow around a car (geometry courtesy of Volvo Car Corporation).

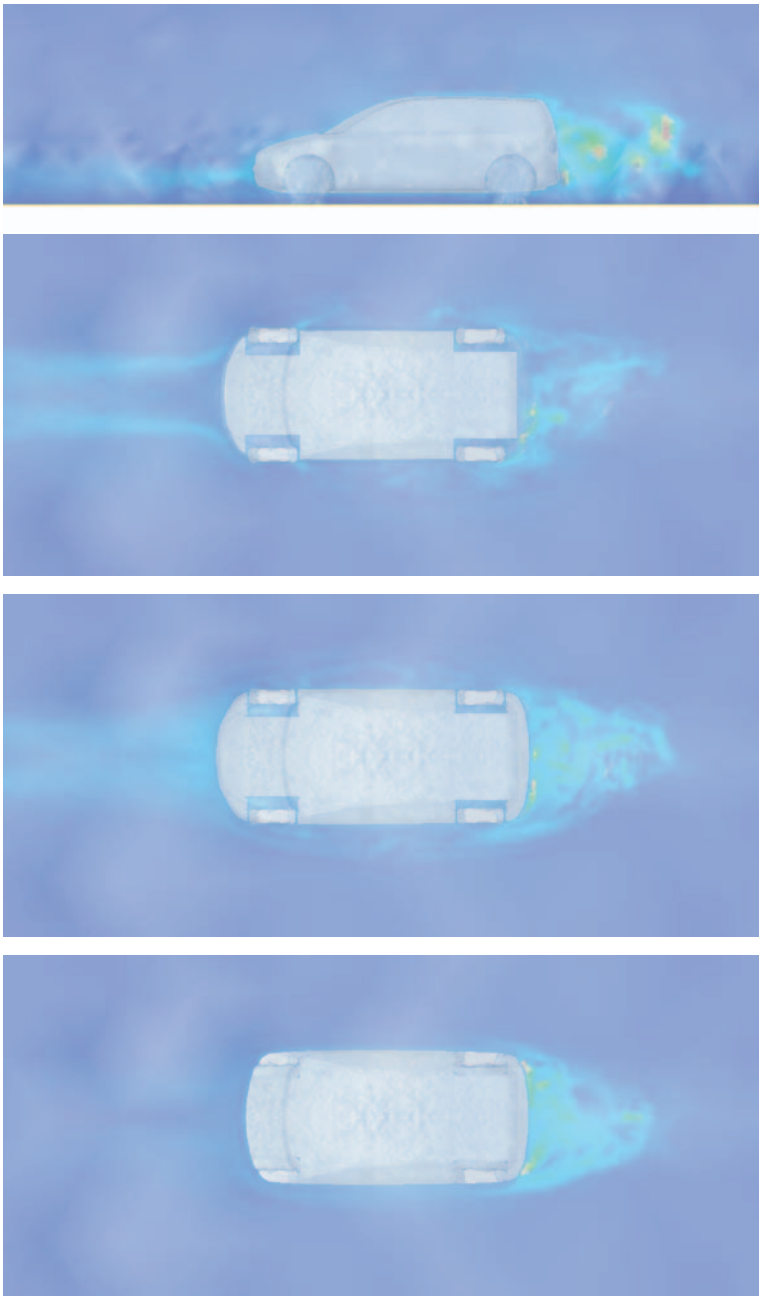

Fig. 1.21. From Chapter 33: dual solution with respect to drag around a car (geometry courtesy of Volvo Car Corporation).

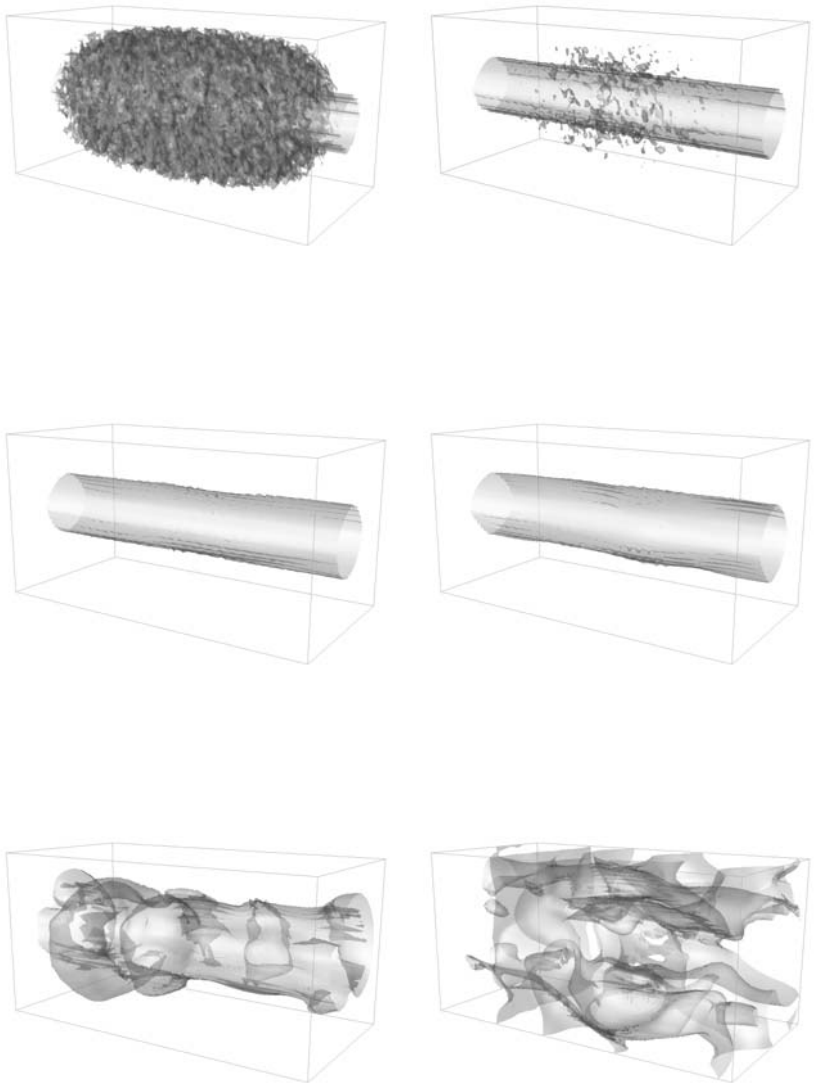

Fig. 1.22. From Chapter 36: streamwise velocity iso-surfaces for $|u_1| = 0.02$ in jet flow (random initial perturbation) for $t = 0, 2, 5, 7, 10, 15$

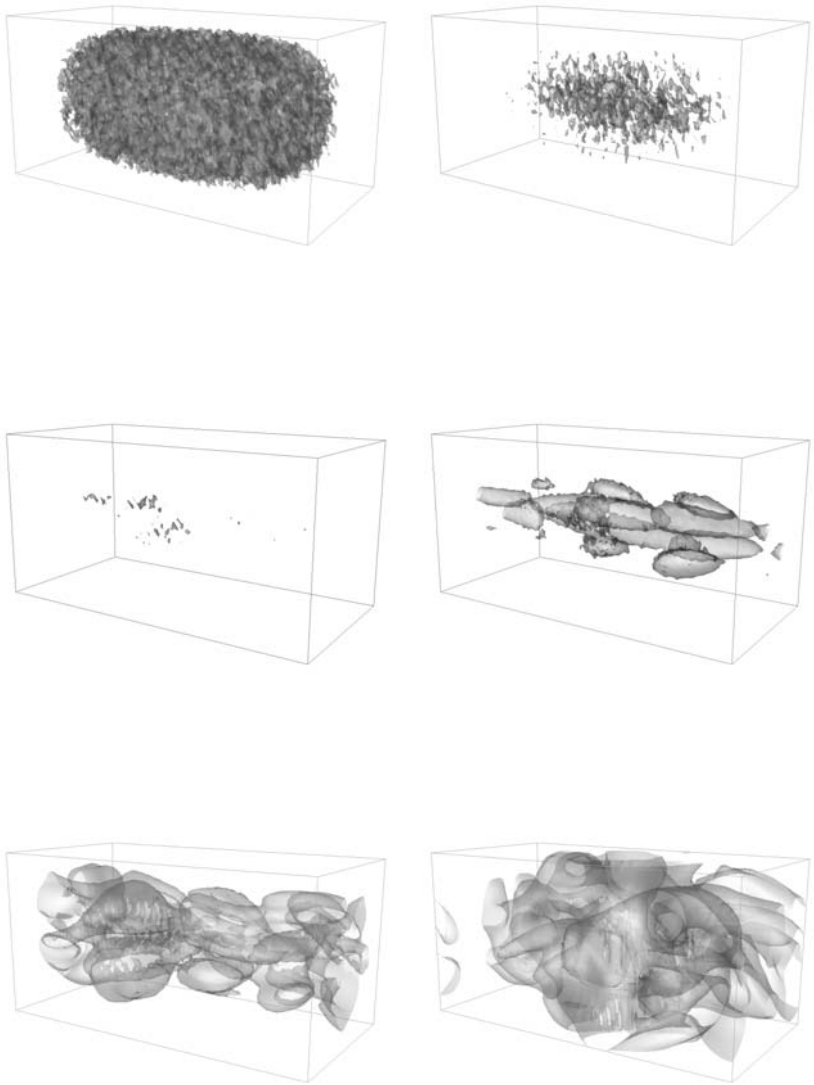

Fig. 1.23. From Chapter 36: Transversal velocity iso-surfaces for $|u_2| = 0.02$ in jet flow (random initial perturbation) for $t = 0, 2, 5, 7, 10, 15$

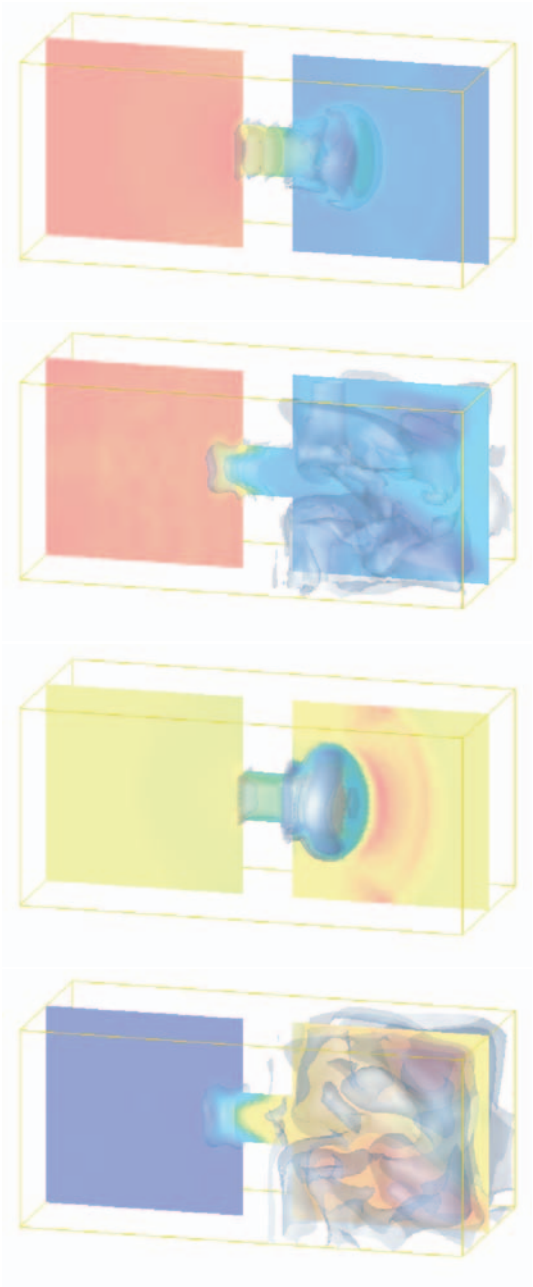

Fig. 1.24. From Chapter 38: EG2 simulation of the Joule-Thomson experiment: snapshots of density (upper 2 figures) and temperature (lower 2 figures) at 2 different time instants.